ISSN: 3007-9640 DOI: https://doi.org/10.70114/acmsr.2026.6.1.P113

Effect of Tool Traversing Speed on Microstructure, Interface and Properties of Al/Steel Friction Stir Welding Lap Joints

Linghang Ma [1, 2, a], Yijun Liu [3, b], Xu Zhang [2, c], Guo Chen [2, d], Yue Xie [2, e], Shikang Gao [1, 2, f *], Weizhao Sun [2, g], and Li Zhou [1, 2, h *]

[1] State Key Laboratory of Precision Welding & Joining of Materials and Structures, Harbin Institute of Technology, Harbin 150001, China;

[2] Shandong Provincial Key Laboratory of Special Welding Technology, Harbin Institute of Technology at Weihai, Weihai 264209, China;

[3] Beijing Institute of Aerospace Systems Engineering, Beijing 100076, China

[a] malinghang@outlook.com, [b] liuyijunthu@foxmail.com, [c] 25S130426@stu.hit.edu.cn,

[d] 13347930991@163.com, [e] sheyue98212@qq.com, [f] hitAkang@163.com, [g] wsunthu@163.com,

[h] zhouli@hitwh.edu.cn

Abstract. The joining of Al/steel is crucial for weight reduction and performance optimization in lightweight structures. This study investigates the microstructure, interface characteristics, and mechanical properties of friction stir lap welded AA6061/Q345D steel joints, elucidating the underlying mechanisms of tool traversing speed. The traversing speed influences both the processing time and heat input, thereby affecting the thickness, morphology, and composition of the interfacial reaction layer. Excessive or insufficient thickness of the interfacial layer at lower or higher speeds, respectively. At a speed of 200 mm/min, grain refinement was observed in the weld zones adjacent to the interface. A continuous intermetallic compound layer approximately 4 μm thick formed at the interface, exhibiting a uniform and planar morphology, and was identified primarily as the Al-rich $FeAl_3$ phase. The mechanical properties of the joints first increased and then decreased with rising traversing speed, which correlated with excessive or insufficient thickness and non‑uniformity of the interfacial layer. The joint fabricated at 200 mm/min shows an optimum shear load of 6.01 kN. These results provide a viable approach for achieving high‑performance solid‑state joints between Al/steel.

Keywords: Dissimilar materials of Al/Steel; Friction stir lap welding; Interface; Microstructure; Mechanical properties

1. Introduction

The joining of Al/steel is of significant importance for reducing structural weight while enhancing performance and material utilization efficiency. Currently, welded aluminum-steel structures are widely employed in industrial applications such as aircraft fuselages and new-energy vehicles [1,2]. However, the substantial differences in the physical and chemical properties of Al/steel lead to poor compatibility in fusion welding technologies [3]. In this context, friction stir welding (FSW) has gained prominence as an effective solid-state process for welding dissimilar materials [4]. By avoiding melting and relying on thermomechanical plasticization, FSW theoretically minimizes the generation of brittle intermetallic compounds (IMCs) while producing sound joints. Friction stir lap welding (FSLW) is particularly suitable for manufacturing lap-style joints common in sheet metal assemblies. The joint interface, where elemental diffusion and bonding occur under friction and stirring-induced thermomechanical effects, represents the critical region governing weld quality. Both tool pin geometry and welding parameters influence heat input and material flow, thereby affecting the joint's microstructure and interface formation [5, 6, 7, 8]. Modifications such as specialized pin features or increased shoulder diameter generally enhance heat generation and material flow during welding, which in turn influences interface characteristics

ISSN: 3007-9640 DOI: https://doi.org/10.70114/acmsr.2026.6.1.P113
and joint integrity [9]. Higher tool rotational speeds typically increase frictional heating and plastic deformation. Likewise, greater penetration depth or direct tool contact with the steel substrate further raises interfacial temperatures [10,11]. Under intense thermomechanical action, metallic fragments and substantial IMCs can form. In Al/steel joints, common IMCs include Fe_3Al, FeAl, and $FeAl_3$, whose formation conditions and influence on weld quality vary with their type, morphology, and distribution [12, 13, 14, 15].

Up to date, the mechanical properties of Al/steel dissimilar joints are known to be governed by their microstructure and interfacial characteristics. However, studies focusing on controlling the interface structure and composition by adjusting the tool traversing speed remain limited. Therefore, this study investigates the microstructure, interface characteristics, and mechanical properties of friction stir lap welded AA6061/Q345D steel joints, aiming to elucidate the underlying mechanisms of effects from various traversing speeds. In the experiment, joints were fabricated at speeds from 50 to 400 mm/min while maintaining the rotational speed and shoulder plunge. The results demonstrate a crucial influence of traversing speed on material mixing and intermetallic compound formation. This study clarifies the relationship between traversing speed, interface evolution, and joint performance, and guides optimizing FSLW parameters to achieve reliable Al/steel joints with enhanced mechanical properties.

2. Methods

2.1 Materials

Commercial AA6061 aluminum plates and Q345D steel plates measuring 150 mm × 100 mm × 3 mm were used. The chemical compositions of AA6061 and Q345D are provided in Table 1.

Table 1. Chemical compositions of base metals (wt.%).

Base Metal	Elements							
	Al	Fe	Si	Mg	Mn	Cu	C	Ni
Q345D	-	Bal.	0.50	-	1.70	0.30	0.18	0.50
AA6061	Bal.	≤0.70	≤0.55	≤1.00	≤0.15	≤0.40	-	-

2.2 Welding and Testing

A schematic illustration of the FSLW process for Al/steel was shown in Fig. 1. During the process, the Q345D steel plate was positioned as the lower substrate. The welding tool, made from a W-Re alloy, had a shoulder diameter of 15 mm. The W-Re alloy tool pin is a cylinder with a diameter of 5 mm and a height of 2.85 mm. To investigate the effect of tool traversing speed on joint microstructure and mechanical properties, the rotational speed and shoulder plunge depth were kept constant at 1000 rpm and 0.2 mm, respectively, while the traversing speed was set to 50, 100, 200, 300, and 400 mm/min. Before welding, all plates were ground and cleaned to ensure weld quality.

After welding, specimens for microstructural and mechanical characterization were sectioned from the locations indicated in Figure 1 using electrical discharge machining. Then, the samples were ground and polished sequentially using sandpaper. Subsequently, chemical etching was performed: Keller's reagent was applied to the AA6061 specimens for 120 s, while the Q345D specimens were etched with a nitric acid-alcohol solution for 10 s. Microstructural observations were conducted using an Olympus optical microscope (OM). The interfacial region was examined with a Zeiss scanning electron microscope (SEM), and its element was analyzed by energy-dispersive X-ray spectroscopy (EDS). Phase identification at the interface was carried out using transmission electron microscopy (TEM). Tensile tests were conducted on an INSTRON 1186 testing machine at a constant speed of 1 mm/min. Microhardness was measured with a load of 9.8 N and a dwell time of 10 s, with test points spaced 0.5 mm apart laterally and 0.25 mm apart

ISSN: 3007-9640 DOI: https://doi.org/10.70114/acmsr.2026.6.1.P113
longitudinally (as indicated in Figure 1). Finally, the fracture morphology of the tensile specimens was observed using SEM.

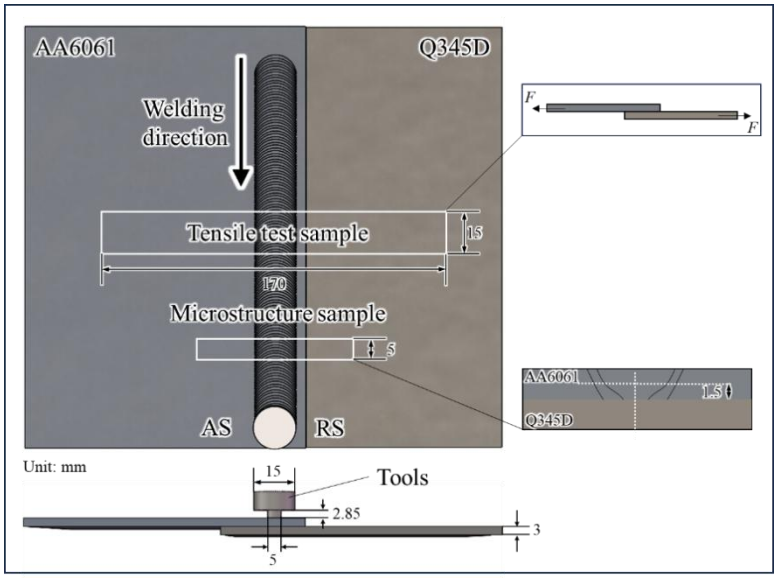


Fig. 1 Configuration of Al/steel FSLW

3. Results and Discussion

3.1 Surface Appearances and Macrostructures

Figure 2 shows the surface and cross-sectional morphologies of AA6061/Q345D friction stir lap welding joints produced at different tool traversing speeds. Due to the excellent weldability of AA6061, all joints were free from macroscopic defects across the tested speed range [16]. However, the linear heat input of the welding process increases as the speed decreases [17]. Higher heat input improves the plastic flow of the aluminum matrix, resulting in more pronounced flash under the rotational and extrusion action of the tool. Moreover, the flash tends to accumulate on the retreating side (RS) of the weld. Notably, at low traversing speeds of 50 and 100 mm/min, the Q345D steel was frictionally stirred and embedded into the AA6061 matrix, forming hook structures at the Al/steel interface. This is directly attributed to the greater heat input at low speeds, which sufficiently softens the base material and allows the tool pin to drag the plasticized material to form hooks. In contrast, at higher traversing speeds, the reduced heat input limits plastic deformation and intermixing of the two materials, yielding a relatively flat Al/steel interface.

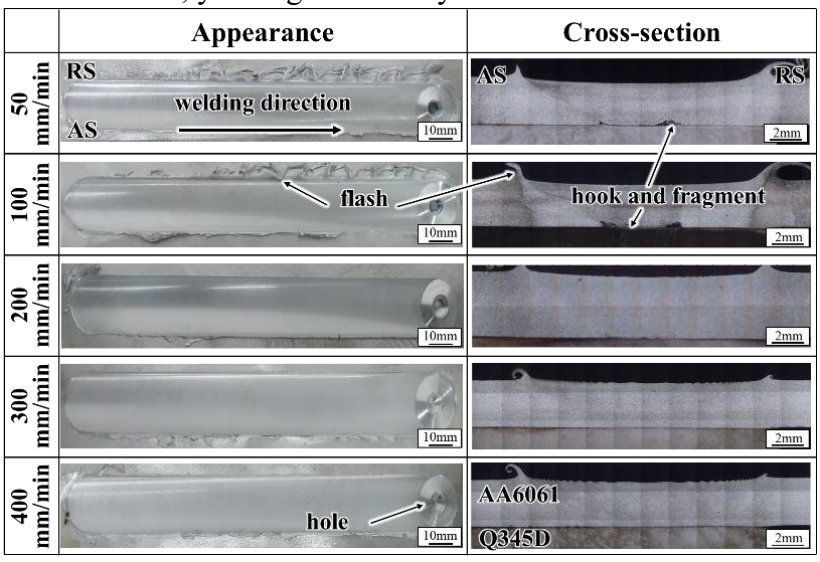


Fig. 2 Surface appearances and macrostructures in cross-section under various traversing speed

ISSN: 3007-9640 DOI: https://doi.org/10.70114/acmsr.2026.6.1.P113

3.2 Grain Microstructure Evolution

Figure 3 presents the microstructure on the steel side of an Al/steel friction stir lap joint fabricated under typical processing parameters. Distinct hook-like features and fragmented steel particles are visible. Figure 3(b) shows an enlarged view of the interfacial region, displaying a mechanically mixed morphology induced by the friction and stirring of the pin. Figures 3(e-g) display metallographic images of the steel at varying distances from the interface. The grain size in the Q345D steel decreases progressively toward the interface. This refinement resulted from the peak temperature exceeding 400°C during welding. The combined friction and heating from the tool pin induced recrystallization in the steel near the interface, leading to significant grain refinement. [18]. Thermomechanical stress was most severe adjacent to the interface and diminished with distance. In regions farther from the interface, the elevated temperature also promoted recovery within the steel, contributing to the observed grain-size gradient [19]. Since the strength of the steel is considerably higher than that of the joint interface, tensile-shear failure did not occur on the steel side. Consequently, variations in the steel microstructure had a negligible influence on joint integrity. Therefore, the microstructural evolution of the steel under different processing parameters was not investigated in subsequent experiments.

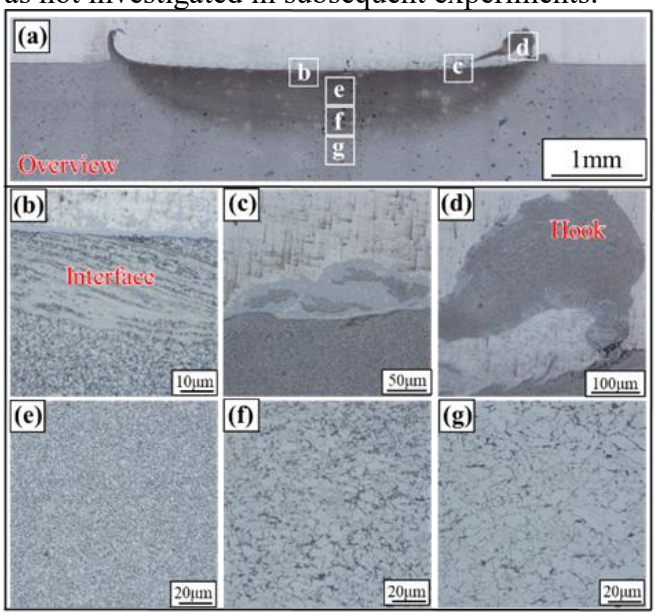


Fig. 3 Morphology of typical parametric joints and microstructure of steel Q345D (a) morphology (b-g) Enlarged view of positions (b-g) in fig. (a)

Figure 4 presents the microstructure on the Al alloy side at various tool traversing speeds. A friction stir weld typically comprises the weld nugget zone (WNZ), the thermomechanically affected zone (TMAZ), and the heat-affected zone (HAZ). Each zone experiences distinct thermal and mechanical histories, resulting in different microstructural characteristics. Within the WNZ, intense frictional heating combined with severe mechanical stirring drives complete dynamic recrystallization of the original grains, forming refined and equiaxed grains [20]. Such uniformly refined microstructures generally possess enhanced load-bearing capacity and plastic deformability [21]. With the traversing speed increasing from 50 to 400 mm/min, the grain size in the WNZ decreased from 10.11 μm to 7.52 μm. This trend is due to the attenuated heat input at higher speeds, which suppresses post-recrystallization grain growth [22]. The TMAZ, located at the side of the weld nugget, experiences intense shear deformation. This results in grains elongated along the nugget boundary. The TMAZ undergoes partial dynamic recrystallization, leading to a mixed microstructure of unrecrystallized, deformed coarse grains and partially recrystallized fine grains, which creates an inhomogeneous grain size distribution. Currently, the high dislocation density accumulated during plastic deformation promotes the formation of numerous low-angle grain boundaries (LAGBs) through dislocation slip and climb. These microstructural features became

ISSN: 3007-9640 DOI: https://doi.org/10.70114/acmsr.2026.6.1.P113
more pronounced with increasing traversing speed. In the HAZ, grains coarsened due to welding thermal exposure, with the extent of grain growth increasing as the speed decreased.

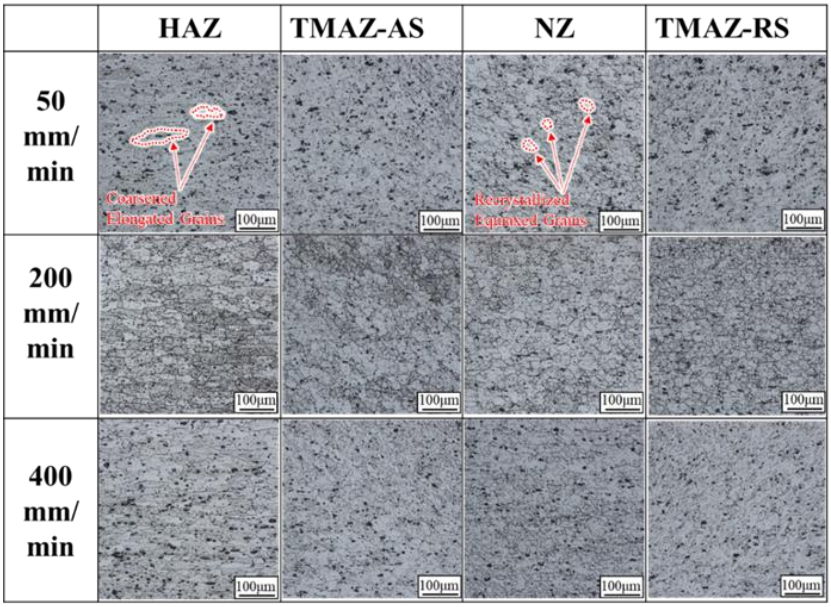


Fig. 4 Microstructure of AA6061 at different traversing speeds

3.3 Interface Characteristic

Figure 5 shows SEM images and EDS elemental maps of the dissimilar Al/Steel interface at different tool traversing speeds. At 50 mm/min, higher heat input during welding caused the steel substrate to be more extensively stirred by the tool pin, forming the thickest intermixing and diffusion layer. The prolonged interaction time per unit length at this lower speed also resulted in intense but irregular material mixing, leading to an inhomogeneous interfacial region [15]. When the traversing speed was increased to 200 mm/min, the reduced heat generation resulted in a narrower Al-Fe transition zone. The shorter interaction time and lower interfacial temperature limited the embedding of steel fragments into the aluminum matrix, indicating that higher traversing speeds restrain atomic interdiffusion and thereby suppress the formation of intermetallic compounds [23]. At the highest speed of 400 mm/min, elemental interdiffusion was further minimized. The mechanical interaction between the tool and the steel surface per unit weld length became weaker, resulting in the thinnest diffusion layer and the most uniform interface morphology.

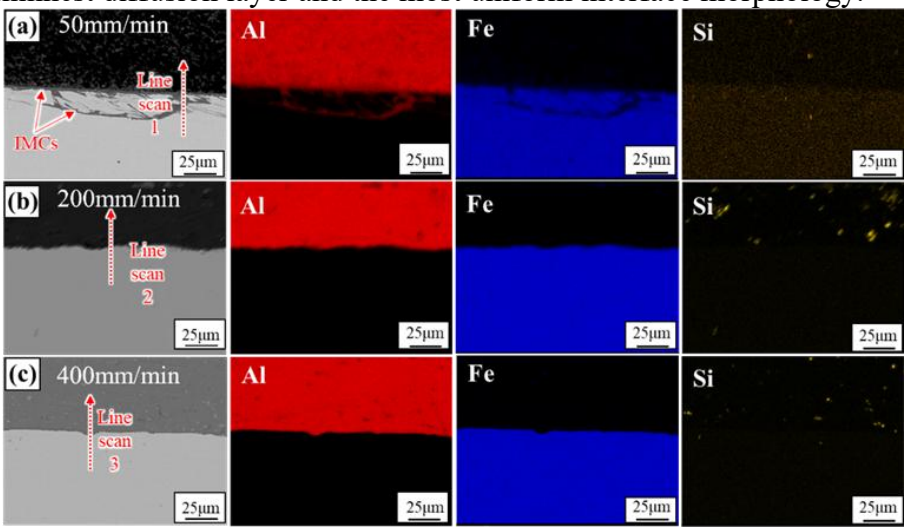


Fig. 5 Mapping scan images of the cross-section at different traversing speed (a) 50 mm/min (b) 200 mm/min (c) 400 mm/min

ISSN: 3007-9640 DOI: https://doi.org/10.70114/acmsr.2026.6.1.P113

To further characterize the interfacial structure, EDS line scans were performed along the paths indicated in Figures 5(a-c), the results are shown in Figure 6. A step size of 0.1 μm was used to accurately resolve the compositions. Figure 6(a) shows the scan results for 50 mm/min. The high heat input and intense mechanical stirring at this speed promoted elemental interdiffusion, resulting in an interfacial layer approximately 26 μm thick. Notably, within a 3 μm region adjacent to the steel substrate, the atomic ratio of Al to Fe approached 1:1, suggesting the formation of an Fe-rich FeAl phase [24]. Toward the aluminum matrix, the Al content increased progressively, with the Al: Fe ratio approaching 3:1, indicating the presence of the $FeAl_3$ phase. Studies indicate that under comparable temperatures, the $FeAl_3$ phase possesses lower free energy and is thus thermodynamically favored during interdiffusion [25]. Furthermore, when the Fe content in the mixture ranges from approximately 10 to 40 at. %, the $FeAl_3$ phase tends to form, while a higher Fe content promotes the formation of the FeAl phase [26]. The lower traversing speed enhanced the intermixing of steel fragments into the Al matrix, creating local regions near the steel side enriched in Fe and facilitating FeAl formation. As the traverse speed increased, the interfacial diffusion layer thickness decreased significantly. At 200 mm/min, the layer measured approximately 4 μm, exhibiting a relatively planar interface with a smoother elemental transition and more uniform intermetallic distribution. At the highest speed, the diffusion layer was thinnest, measuring approximately 2 μm.

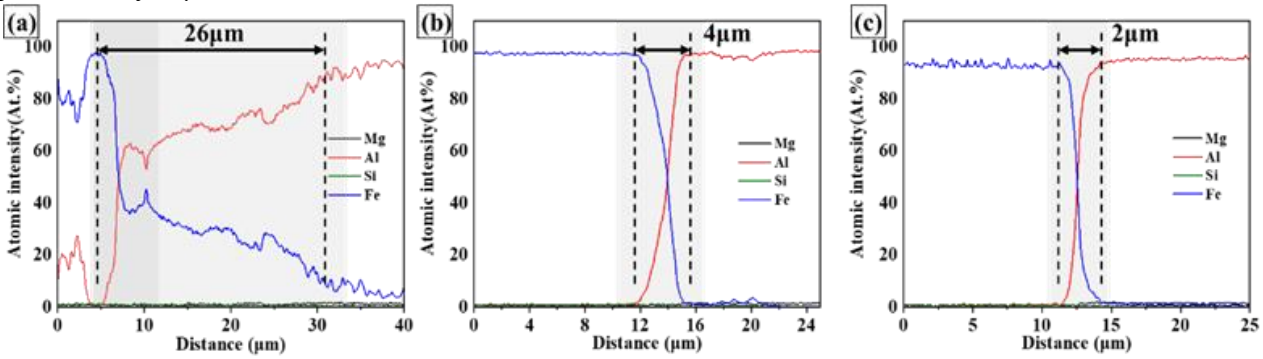


Fig. 6 Line scan image at the marked position in fig.5 (a) 50 mm/min (b) 200 mm/min (c) 400 mm/min

As shown in the TEM image of the 200 mm/min joint (Fig. 7a), the brighter contrast corresponds to the Al, whereas the darker region denotes the steel side. Adjacent to the interface, the steel exhibits refined recrystallized grains, attributable to the thermomechanical processing effect. High-resolution imaging of the interface confirms the formation of IMCs coexisting with the Fe matrix. Selected-area electron diffraction identifies this phase as $FeAl_3$, which is consistent with the EDS results. Figure 7(b) schematically illustrates the interfacial structures obtained under different processing conditions, highlighting the influence of traversing speed on interface evolution. At the speed of 400 mm/min, a thin elemental diffusion layer forms, consisting primarily of Al-rich IMCs. As the speed decreases, the increased frictional stirring per unit length raises the heat input, thereby thickening the diffusion layer and promoting the formation of Fe-rich IMCs. At the lowest speed of 50 mm/min, the thickest diffusion layer develops at the Al/steel interface, along with the incorporation of fragmented and hook into the aluminum matrix and interfacial zone.

ISSN: 3007-9640 DOI: https://doi.org/10.70114/acmsr.2026.6.1.P113

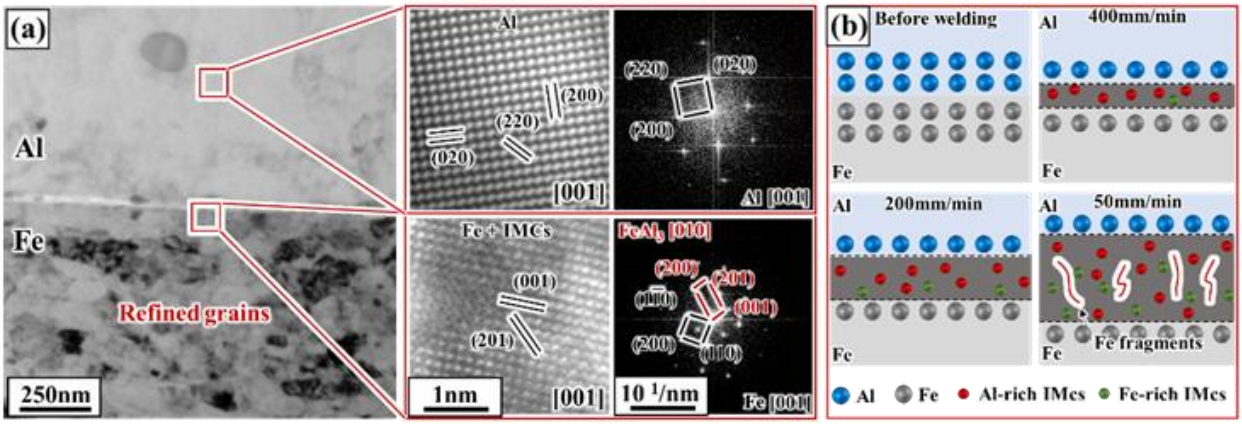


Fig. 7 (a) bright-field interface image at 200 mm/min with high-resolution regional analysis (b) schematic diagram of interface formation

3.4 Microhardness Distribution

Figure 8(a) presents the joint hardness across the middle region of aluminum side at different tool traversing speeds. The profile exhibits the characteristic "W-shaped" pattern typical of FSW aluminum alloys [27]. The lowest hardness was observed in the HAZ, attributed to the presence of incompletely recrystallized grains and the transformation of strengthening phases caused by heat input. [27]. At traversing speeds from 50 to 400 mm/min, the average hardness values in the WNZ zone were 67, 82, 79, 74, and 71 HV, respectively, showing a trend of first increasing and then decreasing with the speed. At lower speeds, higher welding heat promotes grain coarsening in the nugget, reducing hardness. Conversely, excessively high speeds further limit heat input, suppressing the precipitation of strengthening phases and likewise leading to a decrease in hardness [28]. Figure 8(b) shows the hardness distribution along the weld centerline from the steel to the aluminum at various traversing speeds. At speeds of 50 and 100 mm/min, the hardness of the steel adjacent to the interface increased noticeably over a distance of approximately 1 mm. The increasing hardness is due to grain refinement via recrystallization induced by the welding thermal-mechanical cycle. Furthermore, at these lower speeds, the steel may undergo low-temperature tempering within the welding thermal field, contributing to the hardness variation along the thickness direction [19]. When the traversing speed exceeded 200 mm/min, the heat input during the process was lack to induce significant microstructural changes, resulting in slight hardness variation in the steel.

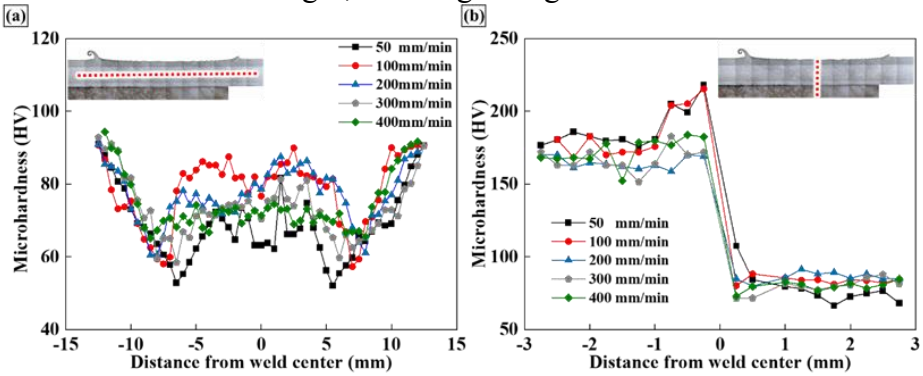


Fig. 8 Microhardness distribution at different traversing speeds (a) vertical distribution (b) horizontal distribution

3.5 Lap Shear Strength

The loading capacity of a lap joint can be used to determine its lap strength. The loading of AA6061/Q345D friction stir lap welds produced at various traversing speeds is illustrated in Fig. 9. The shear load of the joints increases, then decreases with increasing tool traversing speed. The

ISSN: 3007-9640 DOI: https://doi.org/10.70114/acmsr.2026.6.1.P113
optimum shear load of 6.01 kN was obtained at 200 mm/min, whereas relatively low shear loads of 3.26 kN and 3.43 kN were observed at 50 and 400 mm/min, respectively. The variation is mainly influenced by the evolution of the Al/Steel interface characteristics controlled by welding thermal input. At low traversing speeds, the welding process produces an inhomogeneous intermixed interface between aluminum and steel. This results in a thick, brittle IMC layer, such as FeAl, which restricts interfacial deformation [29]. Moreover, the irregular interface morphology induces stress concentration within the softened aluminum matrix during mechanical loading, ultimately leading to the lowest tensile-shear strength. As the speed increases to 200 mm/min, interfacial diffusion becomes more uniform, promoting the formation of a continuous metallurgical bond. Previous studies confirm that optimal joint strength is achieved when the IMC layer thickness remains below approximately 5 μm [4]. Furthermore, it has also been reported that the initially nucleated $FeAl_3$ layer, along with any potentially present high-modulus amorphous phases, can effectively hinder crack propagation, thereby enhancing the shear resistance of the joint [30,31]. When the traversing speed further increases to 400 mm/min, the insufficient thermal input and shortened tool interaction time result in the formation of the thinnest diffusion layer at the interface, leading to relatively weak metallurgical bonding. Nevertheless, the shear load of 3.43 kN remains slightly higher than that at 50 mm/min, which is attributed to the low heat input inhibiting excessive IMC growth and avoiding the formation of an uneven interfacial structure.

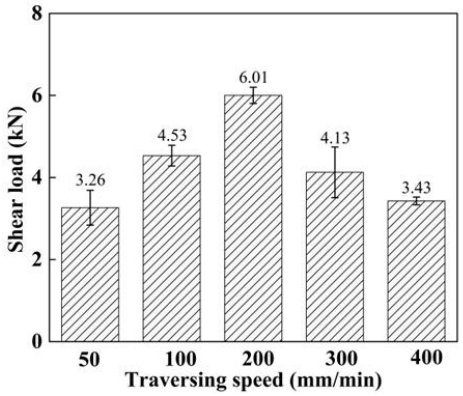


Fig. 9 Shear load at different traversing speeds

3.6 Fracture Behavior

Figure 10 presents the surfaces from tensile-shear fracture samples at different speeds, where (a-c) and (d-f) correspond to the aluminum and steel sides of the fracture, respectively, with associated EDS results summarized in Table 2. At a traversing speed of 50 mm/min, the morphology exhibited a coarse morphology with deep grooves attributable to tool pin action, which is characteristic of failure occurring within the intermetallic compound layer. Higher-magnification observation revealed the fracture surface exhibits a “crack-like” appearance, which is characteristic of brittle fracture morphology [32]. EDS analysis indicated an Al: Fe atomic ratio near 1:2, suggesting that crack propagation proceeded primarily along the FeAl IMC. At 200 mm/min, the fracture surface appeared smoother and displayed finer, more uniform curved markings compared to the lower speed condition. This resulted from the reduced interaction time between the tool and the steel surface, which minimized severe and irregular material intermixing. The fracture surface exhibited a mixed morphology, comprising both dimples and cleavage patterns, indicative of a ductile-brittle characteristic [33]. EDS results suggest that the fracture region consisted of $FeAl_3$ and aluminum phases. Given the inherent brittleness of IMC layers, cracks likely initiated at IMC interfaces and propagated into the adjacent aluminum matrix. At the highest speed of 400 mm/min, the surface was the smoothest, with scarcely visible coarse IMC features or flow patterns. Further magnified examination confirmed a predominantly brittle fracture mode. EDS examination revealed the predominant presence of Fe element on the surface, indicating failure near the Q345D side of the interfacial zone.

ISSN: 3007-9640 DOI: https://doi.org/10.70114/acmsr.2026.6.1.P113

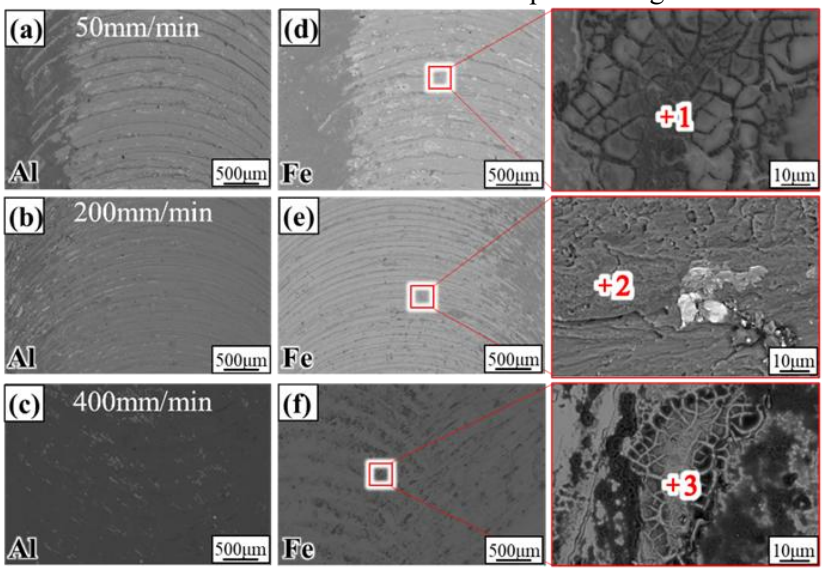


Fig. 10 Fracture morphology at different traversing speeds (a) 50 mm/min (b) 200 mm/min (c) 400 mm/min

Table 2. Point analysis at the marked position in Fig. 10

Point	Elements			Possible Phase
	Al	Fe	Mg	
1	36.94	62.35	0.71	FeAl+Fe
2	75.12	13.29	1.49	Al+$FeAl_3$
3	8.74	91.26	-	Fe

4. Conclusion

In this work, friction stir lap welding of AA6061 and Q345D steel was conducted at varying tool traversing speeds to regulate microstructure and interface characteristics. Their effects on mechanical properties were analyzed. The principal conclusions are as follows:

(1) At a rotational speed of 1000 rpm and a constant shoulder plunge depth of 0.2 mm, Soundly Al/Ti lap joints were produced at speeds from 50 to 400 mm/min. Lower speeds increased linear heat input, promoting flash formation and hook features along the interface due to thermal softening and mechanical interaction with the steel. Higher speeds reduced heat input, resulting in a flatter, more planar Al/steel interface.

(2) The characteristics of the interface exhibited a strong dependence on the heat input. At 50 mm/min, a relatively thick diffusion layer (approximately 26 μm) developed, within which both FeAl and $FeAl_3$ phases were identified. When the speed reached or exceeded 200 mm/min, the diffusion layer became significantly thinner (approximately 4 μm), IMC growth was suppressed, and the layer transitioned into a uniform, continuous morphology, thereby promoting well-interfacial bonding.

(3) Hardness on the aluminum side showed a characteristic "W-shaped" distribution. The hardness within the WNZ initially increased and subsequently decreased with increasing traversing speed. The tensile-shear strength exhibited a similar trend, reaching a peak value of 6.01 kN at a speed of 200 mm/min. This optimum is attributed to a moderate heat input that produced a continuous, suitably thick IMC layer. Conversely, at lower speeds, excessively thick and non-uniform IMC layers weakened the bond, while at higher speeds, overly thin diffusion layers provided insufficient interfacial bond. Both conditions resulted in lower shear loads, about 3.3 and 3.4 kN.

ISSN: 3007-9640 DOI: https://doi.org/10.70114/acmsr.2026.6.1.P113

Acknowledgements

The research was supported by the National Natural Science Foundation of China (No. 52375316).

References

[1] Rhee M H, Song J H, Chung W Y, et al. Joining technology of dissimilar materials for automotive components (II). Journal of Rare Earths, 2004, 22: 35-37.

[2] Bhardwaj N, Narayanan R G, Dixit U S, et al. Recent developments in friction stir welding and resulting industrial practices. Advances in Materials and Processing Technologies, 2019, 5(3): 461-496.

[3] Kuryntsev S. A review: laser welding of dissimilar materials (Al/Fe, Al/Ti, Al/Cu)-methods and techniques, Microstructure and Properties. Materials, 2022, 15(1): 122.

[4] Yang Yue, Luo Zhen, Zhang Yixuan, et al. Dissimilar welding of aluminium to steel: A review. Journal of Manufacturing Processes, 2024, 110: 376-397.

[5] Kaushik P, Dwivedi D K. Effect of tool geometry in dissimilar al-steel friction stir welding. Journal of Manufacturing Processes, 2021, 68: 198-208.

[6] Shamsujjoha M, Jasthi B K, West M, et al. Friction stir lap welding of aluminum to steel using refractory metal pin tools. Journal of Engineering Materials and Technology, 2015, 137(2): 021009.

[7] Saleh M, Morisada Y, Ushioda K, et al. Improvement of weldability and fracture behavior of mild steel and A7075 aluminum alloy dissimilar friction stir welded joints by increasing welding speed. Materials Today Communications, 2023, 37: 107372.

[8] Dehghani M, Amadeh A, Akbari Mousavi S A A. Investigations on the effects of friction stir welding parameters on intermetallic and defect formation in joining aluminum alloy to mild steel. Materials & Design, 2013, 49: 433-441.

[9] Xu Xinli, Zhang Chunwei, Derazkola H A, et al. UFSW tool pin profile effects on properties of aluminium-steel joint. Vacuum, 2021, 192: 110460.

[10] Kumar R, Manjaiah M, Davidson M J. The effect of friction stir welding on the microstructure and mechanical properties of the dissimilar SS304 and Al7075-T6 alloy joints. Welding International, 2023, 37(11): 643-654.

[11] Nandan R, Roy G G, Lienert T J, et al. Three-dimensional heat and material flow during friction stir welding of mild steel. Acta Materialia, 2007, 55(3): 883-895.

[12] Aghajani Derazkola H, Khodabakhshi F. Intermetallic compounds (IMCs) formation during dissimilar friction-stir welding of AA5005 aluminum alloy to St-52 steel: numerical modeling and experimental study. The International Journal of Advanced Manufacturing Technology, 2019, 100(9-12): 2401-2422.

[13] Beygi R, Galvão I, Akhavan-Safar A, et al. Effect of alloying elements on intermetallic formation during friction stir welding of dissimilar metals: A critical review on aluminum/steel. Metals, 2023, 13(4): 768.

[14] Wang Tianhao, Sidhar H, Mishra R S, et al. Evaluation of intermetallic compound layer at aluminum/steel interface joined by friction stir scribe technology. Materials & Design, 2019, 174: 107795.

[15] [15] Zamanzade M, Barnoush A, Motz C. A review on the properties of iron aluminide intermetallics. Crystals, 2016, 6(1): 10.

[16] Ogunsemi B T, Abioye T E, Ogedengbe T I, et al. A review of various improvement strategies for joint quality of AA 6061-T6 friction stir weldments. Journal of Materials Research and Technology, 2021, 11: 1061-1089.

[17] Panda B, Garg A, Jian Z, et al. Characterization of the tensile properties of friction stir welded aluminum alloy joints based on axial force, traverse speed, and rotational speed. Frontiers of Mechanical Engineering, 2016, 11(3): 289-298.

[18] Choi H N, Fujii H, Lee S J. Dynamic recrystallization, textural evolution, and strengthening mechanism of medium-Mn steel subjected to friction-stir welding (FSW). Materials Characterization, 2025, 227: 115307.

ISSN: 3007-9640 DOI: https://doi.org/10.70114/acmsr.2026.6.1.P113
[19] Cui Hongbo, Hu Yawen, Chen Shuai, et al. Control of the microstructural evolution and toughness of welded joints by preheating and subsequent cooling in hybrid friction stir welding of Q960 high strength steel. Materials Today Communications, 2024, 39: 109363.

[20] Yu Pengfei, Wu Chuansong, Shi Lei. Analysis and characterization of dynamic recrystallization and grain structure evolution in friction stir welding of aluminum plates. Acta Materialia, 2021, 207: 116692.

[21] Sun Guangda, Zhou Li, Liu Yuning, et al. Microstructure characterization and evaluation of mechanical properties in 2A97 aluminum-lithium alloys welded by stationary shoulder friction stir welding. Journal of Materials Research and Technology, 2022, 16: 416-432.

[22] Song Jinjiang, Sun Youping, Li Wangzhen, et al. Microstructures, texture evolution and mechanical properties of dissimilar friction stir welded joints 5083-H111/6082-T6 with different welding speeds. Materials Today Communications, 2025, 48: 113480.

[23] Ghiasvand A, Suksatan W, Tomków J, et al. Investigation of the effects of tool positioning factors on peak temperature in dissimilar friction stir welding of AA6061-T6 and AA7075-T6 aluminum alloys. Materials, 2022, 15(3): 702.

[24] Chen C M, Kovacevic R. Joining of Al 6061 alloy to AISI 1018 steel by combined effects of fusion and solid state welding. International Journal of Machine Tools and Manufacture, 2004, 44(11): 1205-1214.

[25] Zhang Ting, Wang Kuaishe, Qiao Ke, et al. Evolution mechanism of intermetallic compounds and the mechanical properties of dissimilar friction stir welded QP980 steel and 6061 aluminum alloy. Materials Characterization, 2023, 202: 113033.

[26] Ma Linghang, Xu Ziyan, Zhang Tao, et al. In-situ formed amorphous phase in aluminum/steel friction stir welds: Interface evolution and strength improvement. Journal of Advanced Joining Processes, 2024, 9: 100220.

[27] Woo W, Choo H, Withers P J, et al. Prediction of hardness minimum locations during natural aging in an aluminum alloy 6061-T6 friction stir weld. Journal of Materials Science, 2009, 44(23): 6302-6309.

[28] Kalinenko A, Kim K, Vysotskiy I, et al. Microstructure-strength relationship in friction-stir welded 6061-T6 aluminum alloy. Materials Science and Engineering: A, 2020, 793: 139858.

[29] Prasad Mahto R, Pal S K. Friction stir welding of dissimilar materials: an investigation of microstructure and nano-indentation study. Journal of Manufacturing Processes, 2020, 55: 103-118.

[30] Ibrahim A B, Al-badour F A, Adesina A Y, et al. Effect of process parameters on microstructural and mechanical properties of friction stir diffusion cladded ASTM A516-70 steel using 5052 Al alloy. Journal of Manufacturing Processes, 2018, 34: 451-462.

[31] Schuh C, Hufnagel T, Ramamurty U. Mechanical behavior of amorphous alloys. Acta Materialia, 2007, 55(12): 4067-4109.

[32] Wu Zhengkai, Toda H, Fujihara H, et al. Long-term reliability of high-zinc Al-Zn-Mg-Cu alloys against stress corrosion cracking. Engineering Failure Analysis, 2025, 182: 110002.

[33] Allison P, Hoarston J B, Strain J, et al. Understanding the influence of heat input and deposition pitch on achieving isotropic tensile behavior in large-scale AM of AA7075 additive friction stir depositions. Additive Manufacturing, 2025, 5(109): 104907.